Analyst

Accepted Manuscript

ROYAL SOCIETY OF CHEMISTRY

www.rsc.org/analyst

Journal Name

ARTICLE

A simple and visible colorimetric method through Zr^{4+}-phosphate coordination for the assay of protein tyrosine phosphatase 1B and its inhibitor screening

Received 00th January 20xx,
Accepted 00th January 20xx

DOI: 10.1039/x0xx00000x

www.rsc.org/

Juan Zhang,[a] Jun Lv,[a] Xiaonan Wang,[a] DefengLi,[a] Zhaoxia Wang*[b] and Genxi Li*[a,c]

Inhibitors of protein tyrosine phosphatase 1B (PTP1B) are promising agents for the treatment of type 2 diabetes and obesity, so a colorimetric method has been established in this work for PTP1B assay and its inhibitor screening. The method is based on the chelation effect of zirconium (Zr^{4+}) ions on phosphate group, which may induce aggregation of 4-aminophenylphosphate-functionalized gold nanoparticles (APP/AuNPs) and the corresponding color change of the testing solution. Owing to the dephosphorylation of PTP1B, the aggregation of AuNPs will be influenced by PTP1B since there is no coordination reactivity between Zr^{4+} ions and 4-aminophenol, the hydrolyzed product of APP catalyzed by the enzyme. Therefore, a simple colorimetric method for the assay of PTP1B activity can be developed. Under the optimized experimental conditions, the ratios of absorbance at a wavelength of 650 nm to that at 522 nm vary linearly with the PTP1B activity within a range from 0.005 to 0.18 U/mL with a lowest detection limit of 0.0017 U/mL. Moreover, using this proposed method, the inhibition effect of 6-chloro-3-formyl-7-methylchromone, betulinic acid, ursolic acid, and sodium orthovanadate on PTP1B activity can be tested with IC_{50} values of 10, 13, 9, and 1.1 μM, respectively. Therefore, this new method not only has a great potential for the detection of PTP1B activity but also for the screening of the inhibitors.

1 Introduction

Diabetes mellitus (DM) is a group of metabolic disorders induced by many etiologies and characterized by hyperglycemia. Two forms of DM, type 1 and type 2, have been identified. Type 2 diabetes mellitus (T2DM) which is caused by insulin resistance resulting in loss of normal glucose homeostasis, accounts for >90% of all diabetes[1]. Protein tyrosine phosphatase 1B (PTP1B), an intracellular phosphatase containing a 37 kD catalytic domain and a 35 amino acid hydrophobic C-terminal sequence, has attracted intensive research in recent years. PTP1B can not only dephosphorylate the insulin receptor and insulin receptor substrate[2] but also dephosphorylate phosphotyrosyl residues of proteins and peptides[3]. As a key negative regulator of the insulin signalling pathways, PTP1B plays important roles in down regulation of insulin and leptin signalling pathway. It is also an established therapeutic target for diabetes and obesity[4, 5], and inhibition of PTP1B is anticipated to become a potential therapeutic strategy to treat T2DM[6]. Several strategies are being pursued to improve the pharmacological properties of PTP1B inhibitors[7]. Therefore, it is of great importance to develop sensitive and effective methods to assay PTP1B and screen its inhibitors.

Currently, several methods have been developed to screen potent and selective PTP1B inhibitors. For instance, UV-vis spectroscopy has been used to identify the PTP1B inhibitors through the detection of absorbance at 405 nm of *p*-nitrophenol released from *p*-nitrophenyl phosphate in the presence of PTP1B[8]. Nevertheless, using this method, the detection will be disturbed when the absorption of inhibitor overlaps with that of 4-nitrophenol[9]. Meanwhile, the specific phosphotyrosyl peptides[10] and 3-nitrophosphotyrosine containing molecules[11] have also been used as PTPs substrates for UV-vis spectroscopic measurement. Moreover, a fluorescence turn-on assay has been developed for highly sensitive detection of PTP1B activity by using calcein as the signaling element[12]. A robust screen have also been established in *Saccharomyces cerevisiae* where growth is dependent on PTP1B catalytic activity[13]. Meanwhile, the knockout mice has also been used to evaluate PTP1B inhibitors in *vivo*[14]. But these methods also have their disadvantages. So, it is still highly required to make extensive efforts so as to develop new method.

Benefiting from the unique optical properties of gold nanoparticles (AuNPs)[15], increasing attention has been paid on AuNPs-based colorimetric assays resulting from its easily designable surface chemistry, technical simplicity, and high sensitivity[16]. At present, AuNPs-based colorimetric methods have been used for detecting different kinds of species like nucleic acids[17, 18], proteins[19-21], and metal ions[22-24]. According to previous reports, the specific interaction of phosphate group with zirconium (Zr^{4+}) ions[25-27] has

[a] Laboratory of Biosensing Technology, School of Life Sciences, Shanghai University, Shanghai 200444, PR China. E-mail: genxili@nju.edu.cn; Fax: +86-21-66137541
[b] Department of Oncology, The Second Affiliated Hospital of Nanjing Medical University, Nanjing 210011, PR China. E-mail: zhaoxiawang88@hotmail.com; Fax: +86-25-58509810
[c] State Key Laboratory of Pharmaceutical Biotechnology, Department of Biochemistry, Nanjing University, Nanjing 210093, PR China. E-mail: genxili@nju.edu.cn; Fax: +86-25-83592510

been applied to develop some methods for the measurement of phosphorylated protein based on specific protein-binding DNA, Zr^{4+}-phosphate coordination, and nanocomposite-based signal amplification[28]. Here we report a new method using Zr^{4+}-phosphate coordination for enzyme activity assay and the inhibitor screening.

Based on the above successful studies, in this work, we propose another strategy to induce the color change of AuNPs, thus to propose a simple colorimetric method to detect PTP1B activity and to screen the inhibitors. In this method, aggregation of AuNPs is designed to be induced by the specific combination between Zr^{4+} ions and phosphate groups of 4-aminophenylphosphate, the PTP1B substrate, which is immobilized on the surface of AuNPs. Since this method can be used in a high-throughput fashion with naked eye or a simple colorimetric reader, it may have great potential applications in the future.

2 Experimental

2.1 Materials and chemicals

Protein tyrosine phosphatase 1B (PTP1B, P6244, human recombinant, expressed in *E. coli*, 30 U/mg), chloroauric acid ($HAuCl_4$•$3H_2O$), trisodium citrate, 3-mercaptopropionic acid (MPA), 6-chloro-3-formyl-7-methylchromone (CFM), betulinic acid (BA), ursolic acid (UA), sodium orthovanadate (Na_3VO_4), zirconium (IV) oxychlorideoctahydrate ($ZrOCl_2$•$8H_2O$), HEPES, and trizma base were purchased from Sigma (Shanghai, China). 4-aminophenylphosphate monosodium salt (APP) was purchased from Shanghai, LKT, Laboratories, Inc (Shanghai, China). All buffers and aqueous solutions were prepared with ultrapure water purified with a Millipore Milli-Q water purification system (Barnstead, USA) to a specific resistance of 18 MΩ·cm.

The PTP1B was firstly dissolved in 100 μL HEPES buffer solution (50 mM, pH 7.2) and then was diluted at different concentrations with Tris-HCl buffer solution (50 mM, pH 7.2). CFM, BA, UA, Na_3VO_4, and $ZrOCl_2$•$8H_2O$ were dissolved in aqueous solutions.

2.2 Preparation of AuNPs

AuNPs were synthesized according to the previous study[29]. Briefly, trisodium citrate aqueous solution (10 mL, 38.8 mM) was added to a boiling solution of $HAuCl_4$ (100 mL, 1 mM), and the solution was kept continuously boiling for another 30 min to give a wine red mixture. The mixture was cooled to room temperature and stored in a refrigerator at 4°C

2.3 Synthesis of APP/ AuNPs

MPA was dissolved in aqueous solutions to obtain its final concentration of 2.3 mM. Then, under stirring conditions, 1 mL MPA solution was added to 40 mL AuNPs solution overnight at 25 °C to produce intermediate product, MPA/AuNPs[30]. Subsequently, 1 mL APP aqueous solution (2.6 mM) was mixed with 40 mL

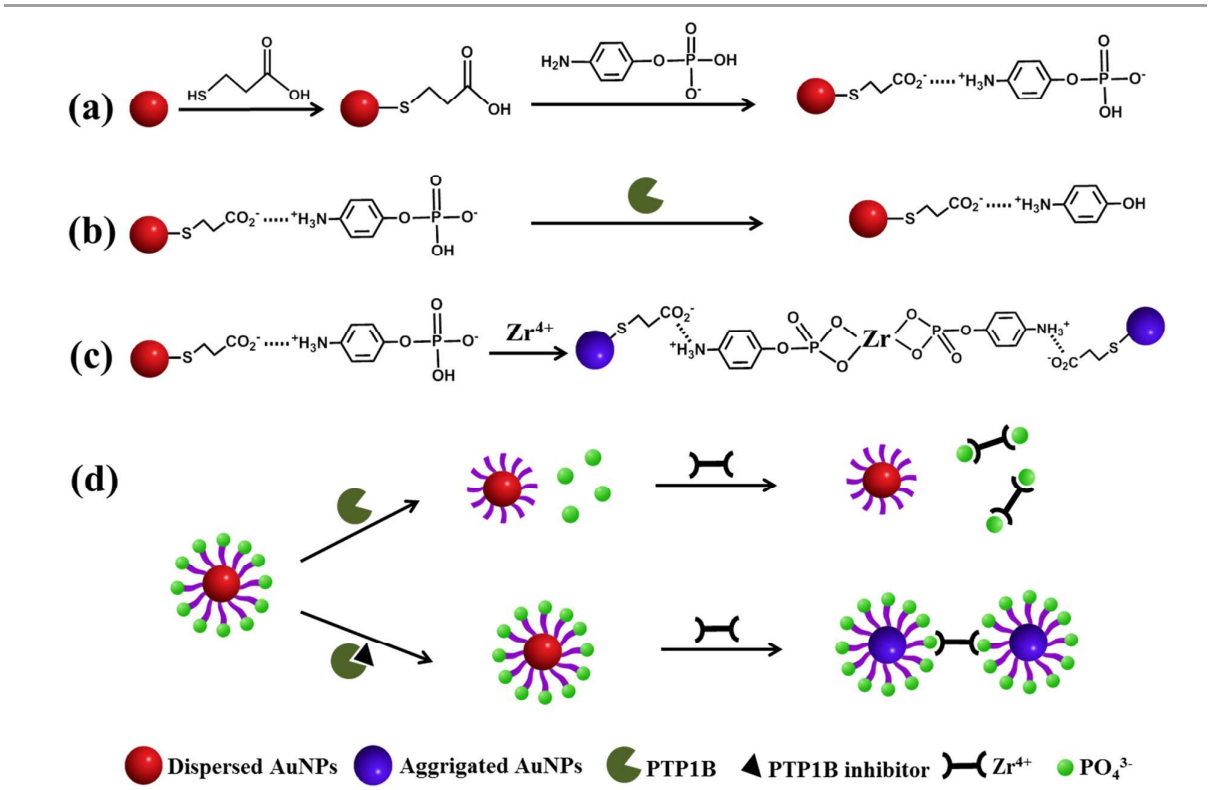

Scheme 1 Schematic illustration of the mechanisms for (a) the synthesis of APP/AuNPs, (b) PTP1B catalyzed reaction, (c) AuNPs aggregation induced by specific coordination between Zr^{4+} ions and phosphate group, (d) colorimetric determination of PTP1B activity and the inhibitor.

MPA/AuNPs solution with continuous stirring for 12 h at 25 °C to obtain the final product, APP/AuNPs.

2.4 PTP1B activity assay

The PTP1B activity assay was performed using the following procedure. The PTP1B was firstly dissolved in 100 μL HEPES buffer solution (50 mM, pH 7.2) and then was diluted at different concentrations with Tris-HCl buffer solution (50 mM, pH 7.2). After that, 10 μL of enzyme solution with different concentrations ranging from 0.005 to 0.18 U/mL was added to 80 μL of dispersed APP/AuNPs solution and the resulting mixture was allowed to stand at 30 °C for 20 min. Then, 10 μL $ZrOCl_2$•$8H_2O$ solution was added to the resulting mixture at room temperature. After 5 min, the reaction solutions were photographed and used for UV-vis spectroscopic measurements.

2.5 Evaluation for Inhibitor assay

For the inhibition assay, CFM, BA, UA, or Na_3VO_4 aqueous solutions (10 μL) with different concentrations were first premixed with PTP1B (10 μL, 0.15 U/mL) for 10 min at 30 °C. Then APP/AuNPs (80 μL) was added to the mixed solution with further incubation for 20 min at 30 °C. After that, the solution of $ZrOCl_2$•$8H_2O$ (10 μL) was added to the resulting mixture to give a final concentration of 0.6 mM. Finally, the reaction solution was allowed to stand at room temperature for 5 min. The absorbance of each sample was recorded using UV-vis spectroscopy and the IC_{50} value calculated. The inhibitory ratios (%) of CFM, BA, UA, or Na_3VO_4 are expressed as follows:

$$\text{Inhibitory ratio}\,(\%) = \frac{A_{650}/A_{522} - A^{*}_{650}/A^{*}_{522}}{A^{0}_{650}/A^{0}_{522} - A^{*}_{650}/A^{*}_{522}} \times 100\,\%$$

where A_{650}/A_{522} is the ratio of the absorbance value at 650 nm to that at 522 nm in the presence of both the inhibitor and the enzyme, and A^{*}_{650}/A^{*}_{522} is the ratio of the absorbance value at 650 nm to that at 522 nm with enzyme only. A^{0}_{650}/A^{0}_{522} is the ratio of the absorbance value at 650 nm to that at 522 nm without enzyme and inhibitor.

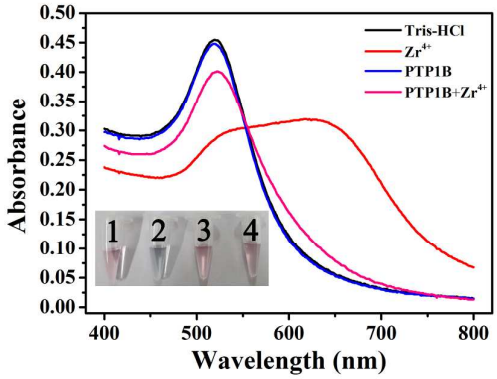

Fig. 1 UV-vis spectra and photographs (inset) of the mixtures prepared by separate addition of Tris-HCl buffer (20 μL, 50 mM, pH 7.2) (vial 1, black curve), $ZrOCl_2$•$8H_2O$ solution (10 μL, 6 mM) (vial 2, red curve), PTP1B (10 μL, 0.15 U/mL) (vial 3, blue curve), or PTP1B (10 μL, 0.15 U/mL) + $ZrOCl_2$•$8H_2O$ solution (10 μL, 6 mM) (vial 4, pink curve) into APP/AuNPs (80 μL) to obtain the final volume of 100 μL with the addition of Tris-HCl buffer.

3 Results and discussions

Different strategies have been developed to induce aggregation of AuNPs. The report DNA can link the oligonucleotides that are modified onto the surface of AuNPs to form DNA-cross-linked AuNPs aggregates based on the complementary base pairing of DNA single-strand[31]. Negatively charged AuNPs will aggregate under a certain concentration of salt through the electrostatic interaction[32]. The aggregation of AuNPs can also be triggered by the formation of covalent bond[30]. Host-guest recognition can also be used for AuNPs aggregation[33]. Additionally, the occurrence of coordination bond has been utilized to induce aggregation of AuNPs[34]. Here we establish a new method based on AuNPs aggregation induced by Zr^{4+}-phosphate coordination for enzyme activity assay and the inhibitor screening. The principle of the colorimetric method is shown in Scheme 1. Firstly, MPA is linked to AuNPs through the formation of Au-S bond. Then enzyme substrate, APP, is further covered on the surface of the modified AuNPs via electrostatic interaction, to give APP/AuNPs (Scheme 1(a)). As shown in FT-IR spectra (Figure S1), the band at 3413 cm^{-1} can be attributed to NH stretching in the APP structure. APP also exhibits three characteristic bands at 1644 cm^{-1}, 1569 cm^{-1}, and 1525 cm^{-1}, belonging to aromatic skeletal vibration. Moreover, the absorption band at 1071 cm^{-1} can be explained for P=O stretching. For the spectrum of APP/AuNPs, the absorption bands at 3434 cm^{-1}, 1644 cm^{-1}, and 1078 cm^{-1} well demonstrate the existence of APP at the outer layer of AuNPs. Subsequently, the addition of Zr^{4+} ions as a linker can trigger the aggregation of AuNPs due to the high coordination reactivity between Zr^{4+} ions and phosphate groups at outer layer of APP/AuNPs (Scheme 1(c)). However, in the presence of PTP1B, the aggregation will not occur as a result of the specific cleavage of APP into 4-aminophenol (AP) which has no binding ability with Zr^{4+} ions (Scheme 1(b)). Since the concentration of the PTP1B is related to the degree of aggregation of AuNPs, a new method for monitoring PTP1B activity through the change in the UV-vis spectrum of the AuNPs dispersion, or even through direct observation by the naked eye can be developed. Moreover, this method can also be used to evaluate PTP1B inhibitors (Scheme 1(d)).

3.1 Mechanism investigation for PTP1B activity assay

As exhibited in Fig. 1, upon addition of Tris-HCl buffer into the APP/AuNPs solution as a control experiment, the red color of the test solution remains unchanged. Meanwhile, the solution shows an obvious absorption at 522 nm (vial 1, black curve), representing the state of well-dispersed AuNPs[35]. The addition of Zr^{4+} ions into the APP/AuNPs solution essentially results in an observable aggregation of AuNPs, leading to a change of the color from the initial wine red to blue, and the production of a new absorption peak at 650 nm (vial 2, red curve). It indicates the occurrence of specific coordination between Zr^{4+} ions and phosphate groups on the surface of APP/AuNPs, which is responsible for the changes in both the color and the UV-vis spectrum of the aqueous dispersion of the AuNPs. With the addition of PTP1B (vial 3, blue curve) into the AuNPs, no apparent aggregation occurs and the test solution keeps the initial

color and exhibits UV−vis spectrum characteristics of well dispersed AuNPs. These results suggest that the addition of PTP1B alone does not induce the aggregation of AuNPs. Moreover, after the addition of PTP1B and Zr^{4+} ions into the solution of APP/AuNPs, both the color and the UV-vis spectrum of the solution remain almost unchanged (vial 4, pink curve), suggesting the negligible aggregation of AuNPs. This phenomenon can be attributed to the cleavage of APP/AuNPs into the corresponding product, AP/AuNPs, catalyzed by PTP1B (Scheme 1(b)), and the latter cannot specifically combine with Zr^{4+} ions due to disappearance of phosphate groups.

3.2 Kinetic analysis for Zr^{4+} ions binding with APP/AuNPs

The mechanism of the specific recognition between Zr^{4+} ions and phosphate groups is displayed in Scheme 1(c). In the presence of Zr^{4+} ions, phosphate groups on the surface of AuNPs can coordinate with Zr^{4+} ions, causing the aggregation of AuNPs. Hence, the concentration of Zr^{4+} ions in the reaction solution will have an obvious influence on the sensitivity of the detection, and the effect of Zr^{4+} ions concentration on the detection system has been further investigated. The UV-vis spectra of the reaction solution have been successively recorded for 30 min after the addition of Zr^{4+}ions with different concentrations. According to previous reports, the ratio of A_{650} to A_{520} can be considered as an indicator of the degree of dispersion/aggregation state of AuNPs[36-38]. Fig. 2(a) shows the time-dependent A_{650}/A_{522} values from the UV-vis spectra of AuNPs in the presence of different concentrations of Zr^{4+} ions in order to estimate the kinetics of the coordination between Zr^{4+} ions and phosphate groups. The A_{650}/A_{522} values increase with increasing concentrations of Zr^{4+} ions. Furthermore, the color of the aqueous dispersions of the AuNPs gradually changes from wine red to violet (right, from vial 1 to vial 12) at the time point of 30 min when the concentrations of Zr^{4+} ions increase from 0 to 0.75 mM. These results indicate that AuNPs aggregation becomes faster with increasing Zr^{4+} ions concentrations in the testing solution. The initial reaction rate (V_0) can be reached by calculating the slopes of the initial part of the kinetic curves of different Zr^{4+} ions concentrations (Fig. 2(b)). With the increase of Zr^{4+} ions concentrations from 0.25 to 0.75 mM, the

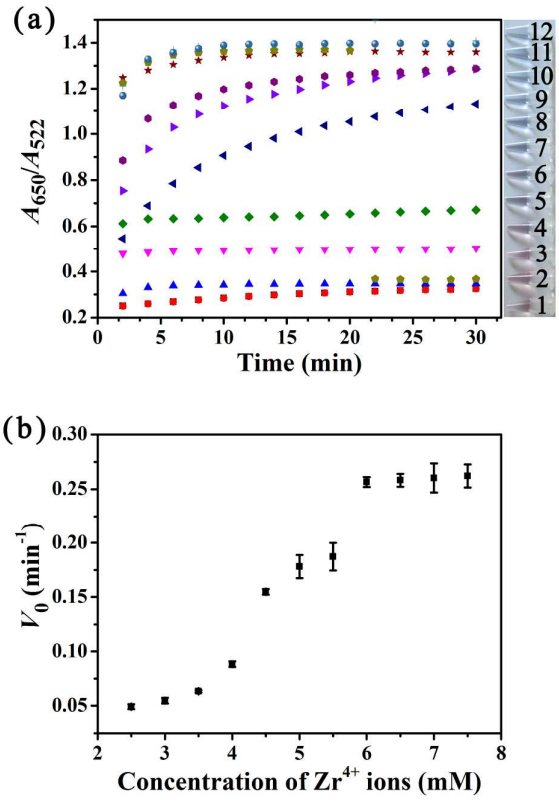

Fig. 2 (a) Kinetic plots of time-dependent A_{650}/A_{522} values versus those with different concentrations of Zr^{4+} ions. Digital photographs at a time point of 30 min after the addition of different concentrations of Zr^{4+} ions are shown on the right. Right, from vial 1 to vial 12: the concentrations of Zr^{4+} ions are 0, 0.25, 0.3, 0.35, 0.4, 0.45, 0.5, 0.55, 0.6, 0.65, 0.7, and 0.75 mM. (b) Initial rate of coordination reaction (V_0) versus Zr^{4+} ions concentration.

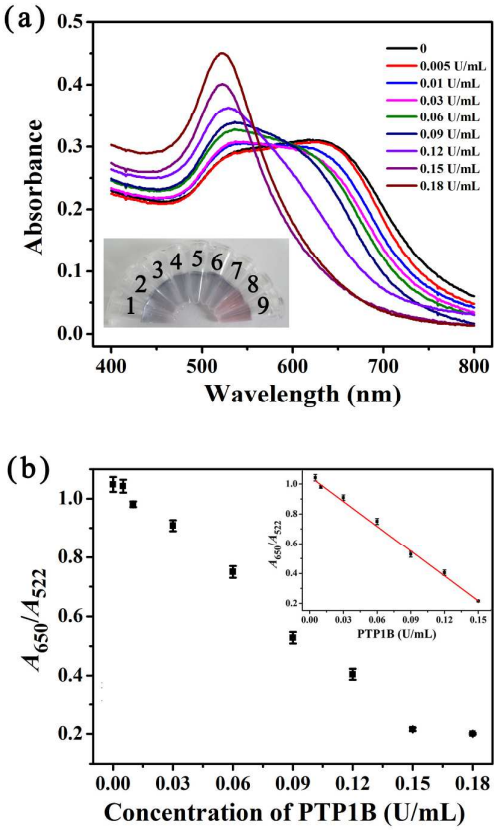

Fig. 3(a) UV-vis spectra and photographs (inset) of the mixtures prepared by the addition of various concentrations of PTP1B (10 μL) into the dispersion of APP/AuNPs followed by the addition of $ZrOCl_2 \bullet 8H_2O$ solution (10 μL, 6 mM). Inset, from vial 1 to vial 9: the PTP1B concentrations were 0, 0.005, 0.01, 0.03, 0.05, 0.07, 0.09, 0.12, 0.15 and 0.18 U/mL. (b) Calibration curve corresponding to A_{650}/A_{522} against the concentrations of PTP1B. Inset shows the linear relationship between the A_{650}/A_{522} values and the concentrations of PTP1B.

initial reaction rate gradually increases. When the concentration of Zr^{4+} ions reaches 0.6 mM, the changes in the rate become less marked. Moreover, the final A_{650}/A_{522} values remain almost unchanged when the concentration of PDBA varies from 0.6 to 0.75 mM (Fig. 2(b)). Therefore, we finally chose 0.6 mM as the optimal reaction concentration of Zr^{4+} ions. In the detection system, this relatively high concentration is used to make the assay rapid, since a high concentration Zr^{4+} ion can make the aggregation of AuNPs very fast.

3.3 PTP1B activity assay

As shown in Fig. 3(a), with the increase of the PTP1B concentrations from 0 to 0.18 U/mL, the color of the dispersion gradually turns from violet to wine red (from vial 1 to vial 9), and a dramatic change occurs in the UV–vis spectra of the dispersion. It should be noticed that with increasing concentration of PTP1B, A_{650} decreases, while A_{522} increases. It can be attributed to the departure of phosphate group at the outer layer of AuNPs as a result of the cleavage of APP into AP under PTP1B catalysis, leading to a

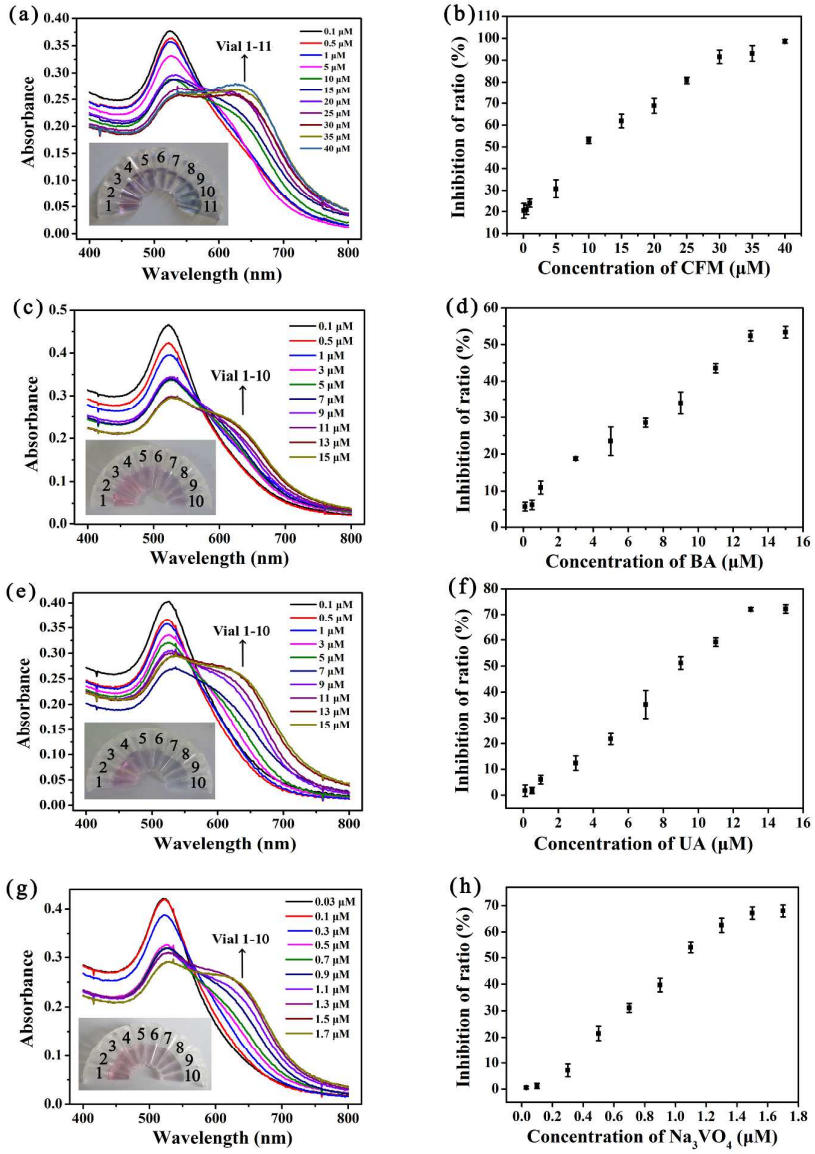

Fig. 4 UV–vis spectra and photographs (inset) of the dispersion upon analyzing various concentrations of (a) CFM, (c) BA, (e) UA and (g) Na_3VO_4. Inset (a), vial 1 to vial 11: the CFM concentrations were 0.1, 0.5, 1, 5, 10, 15, 20, 25, 30, 35, and 40 μM. Inset (c), vial 1 to 10: the BA concentrations were 0.1, 0.5, 1, 3, 5, 7, 9, 11, 13, and 15 μM. Inset (e), vial 1 to 10: the UA concentrations were 0.1, 0.5, 1, 3, 5, 7, 9, 11, 13, and 15 μM. Inset (g), vial 1 to 10: the Na_3VO_4 concentrations were 0.03, 0.1, 0.3, 0.5, 0.7, 0.9, 1.1, 1.3, 1.5, and 1.7 μM. Inhibition ratio versus the concentration of inhibitors: (b) CFM, (d) BA, (f) UA, and (h) Na_3VO_4.

decrease in the extent of the aggregation of the AuNPs.

The calibration curve obtained for the quantitative detection of PTP1B activity with different concentrations of PTP1B is exhibited in Fig. 3(b). In the range from 0 to 0.18 U/mL, the A_{650}/A_{522} values increase with the increasing concentrations of PTP1B. Furthermore, the ratios of A_{650}/A_{522} show a linear response toward PTP1B concentrations ranging from 0.005 U/mL to 0.18 U/mL, and follows the regression equation of $A_{650}/A_{522} = -5.54973C + 1.04973$ (U/mL, $R^2 = 0.998$). Furthermore, the detection limit has also been calculated to be 0.0017 U/mL by the interpolation of the mean plus three times the standard deviation of the zero standards. The detection precision has been investigated according to the slope of the regression of PTP1B (from 0.005 to 0.15 U/mL) obtained from three independent assay processes. The *RSD* of the three slopes is 1.57 %, suggesting that the proposed method has good precision.

3.4 Evaluation for Inhibitor assay

It has been reported that the loss of PTP1B activity can enhance sensitivity towards insulin and resistance to obesity, indicating that a potent active PTP1B inhibitor could be a potential agent for the treatment of T2DM and obesity[39-41]. In order to test and verify that the developed method can be applied for the screening of PTP1B inhibitors, four compounds, CFM, BA, UA, and Na_3VO_4 have been selected for this study.

As exhibited in Fig. 4(a), with increasing CFM concentrations from 0.1 to 40 μM, the color of the AuNPs changes from wine red to violet (inset (a), from vial 1 to vial 11), corresponding to a decrease in A_{522} and an increase in A_{650}. The value of A_{650}/A_{522} first increases gradually with increasing concentrations and then levels off when the inhibitor concentration reaches a certain level, indicating that the inhibition by CFM has a dose dependent process. It has been reported that CFM incorporating the phosphate-mimicking functional fragment can competitively inhibit PTP1B activity[42]. Hence, CFM and APP/AuNPs can competitively bind the active site of PTP1B so as to prevent the cleavage of APP into AP by the enzyme and promote the aggregation of AuNPs. Moreover, it is found that 30 μM CFM can significantly inhibit PTP1B activity because there is no evident change in either the UV-vis spectra or the color of the dispersion (Fig. 4(a), from vial 8 to vial 10). Furthermore, the maximum inhibition ratio of CFM is 98.06 % with the IC_{50} value of 10 μM (Fig. 4(b)), which is in accordance with the values reported previously[42].

Different from those of CFM, BA inhibits PTP1B activity through a mixed noncompetitive and anticompetitive mode[43], so it was also used to evaluate the proposed assay method. As shown in Fig. 4(c), with the increase of BA concentrations from 0.1 to15 μM, the color of the dispersion gradually turns from wine red to purple (inset (c), from vial 1 to vial 10), corresponding to the observed decrease in A_{522} and the increase in A_{650}. It is observed that the activity of 0.15 U/mL PTP1B can be significantly inhibited by the addition of 13 μM BA, since no obvious change in either UV-vis spectra or the color of the dispersion can be observed (Fig. 4(c), from vial 9 to vial 10). The maximum inhibition ratio of BA is 54.51 %, with an IC_{50} value of 13 μM (Fig. 4(d)), consistent with the previous report[43].

UA has been demonstrated time-independent inhibition of PTP1B with typical characteristics of a competitive inhibitor[44]. As depicted in Fig. 4(e), with the increase of UA concentrations from 0.1 to 15 μM, the color of the dispersion gradually changes from wine red to purple (inset (e), from vial 1 to vial 10), corresponding to the observed decrease in A_{522} and the increase in A_{650}. The activity of 0.15 U/mL PTP1B can be obviously inhibited when the UA concentration reaches 13 μM, because that there is no clear change in either UV-vis spectra or the color of testing solution (Fig. 4(e), from vial 8 to vial 10). The maximum inhibition ratio of UA is 73.35 %, with an IC_{50} value of 9 μM (Fig. 4(f)), in agreement with the previous report[44].

Na_3VO_4 is generally thought to bind as a transition state analog to the phosphoryl transfer enzymes, so it has been considered as a common competitive inhibitor for PTP1B[45]. As illustrated in Fig. 4(g), with the increasing Na_3VO_4 concentrations from 0.03 to 1.7 μM, the color of the dispersion gradually changes from wine red to violet (inset (g), from vial 1 to vial 10), corresponding to the decrease of absorbance at 522 nm and the increase of absorbance at 650 nm. It should be noticed that upon adding 1.5 μM Na_3VO_4, PTP1B activity can be apparently inhibited as a result of no obvious change in either UV-vis spectra or the color of the testing solution (Fig. 4(g), from vial 9 to vial 10). The maximum inhibition ratio of Na_3VO_4 is 69.59 %, with an IC_{50} value of 1.1 μM (Fig. 4(h)), in accordance with the previous report[46].

In a word, these results demonstrate that the developed colorimetric method can be used to evaluate the PTP1B inhibitor efficiency. However, there are some limitations of this system. For example, the inhibitors containing chelating moiety with Zr^{4+} ion can not be well screened by using the proposed method.

4 Conclusions

A simple, visible, and effective colorimetric method has been established for PTP1B activity assay and the inhibitor screening based on the Zr^{4+} ions binding to phosphate group through chelation using APP/AuNPs. The method owns the advantages in terms of its low technical and instrumental demands, simple, and rapid operation. Above all, this method has a great potential for the practical detection of PTP1B activity and the effective screening of inhibitors.

Acknowledgements

This work is supported by the National Natural Science Foundation of China (Grant Nos. 31101354 and 21235003) and the Innovation Program of Shanghai Municipal Education Commission (No. 15ZZ048).

References

1 Z. Q. Liu, T. Liu, C. Chen, M. Y. Li, Z. Y. Wang, R. S. Chen, G. X. Wei, X. Y. Wang and D. Q. Luo, *Toxicol. Appl. Pharm.*, 2015, **285**, 61-70.
2 H. Ding, Y. Zhang, C. Xu, D. Hou, J. Li, Y. Zhang, W. Peng, K. Zen, C. Y. Zhang and X. Jiang, *Diabetologia*, 2014, **57**, 2145-2154.
3 H. Lee, J. S. Yi, A. Lawan, K. Min and A. M. Bennett, *Semin. Cell Dev. Biol.*, 2015, **37**, 66-72.
4 A. Haque, J. N. Andersen, A. Salmeen, D. Barford and N. K.

Tonks, *Cell*, 2011, **147**, 185-198.
5 A. A. Lanahan, D. Lech, A. Dubrac, J. Zhang, Z. W. Zhuang, A. Eichmann and M. Simons, *Circulation*, 2014, **130**, 902-909.
6 J. Z. Liu, S. E. Zhang, F. Nie, Y. Yang, Y. B. Tang, W. Yin, J. Y. Tian, F. Ye and Z. Xiao, *Bioorg. Med. Chem. Lett.*, 2013, **23**, 6217-6222.
7 Y. Kurogi and O. F. Guner, *Curr. Med. Chem.*, 2001, **8**, 1035-1055.
8 Q. H. Vo, P. H. Nguyen, B. T. Zhao, M. Y. Ali, J. S. Choi, B. S. Min, T. H. Nguyen and M. H. Woo, *Fitoterapia*, 2015, **103**, 113-121.
9 Y. Sawada, T. Tsuno, T. Ueki, H. Yamamoto, Y. Fukagawa and T. Oki, *J. Antibiot.*, 1993, **46**, 507-510.
10 Q. Xiao, R. Luechapanichkul, Y. Zhai and D. Pei, *J. Am. Chem. Soc.*, 2013, **135**, 9760-9767.
11 J. V. Ameijde, J. Overvoorde, S. Knapp, J. D. Hertog, R. Ruijtenbeek and R. M. Liskamp, *Anal.Biochem.*, 2014, **448**, 9-13.
12 C. Liu, F. Wang, Y. Wang and Z. Li, *Chem. Commun.*, 2014, **50**, 13983-13986.
13 J. Montalibet and B. P. Kennedy, *Biochem. Pharmacol.*, 2004, **68**, 1807-1814.
14 C. Dufresne, P. Roy, Z. Wang, E. A. Appiah, W. Cromlish, Y. Boie, F. Forghani, S. Desmarais, Q. Wang, K. Skorey, D. Waddleton, C. Ramachandran, B. P. Kennedy, L. Xu, R. Gordon, C. C. Chan and Y. Leblanc, *Bioorg. Med. Chem. Lett.*, 2004, **14**, 1039-1042.
15 T. Sumi, S. Motono, Y. Ishida, N. Shirahata and T. Yonezawa, *Langmuir*, 2015, **31**, 4323-4329.
16 Y. Zhou, H. Dong, L. Liu, M. Li, K. Xiao and M. Xu, *Sensor. Actuat. B-Chem.*, 2014, **196**, 106-111.
17 X. Mao, A. Gurung, H. Xu, M. Baloda, Y. He and G. Liu, *Anal. Sci.*, 2014, **30**, 637-642.
18 C. Ma, W. Wang, A. Mulchandani and C. Shi, *Anal. Biochem.*, 2014, **457**, 19-23.
19 M. Lepoitevin, M. Lemouel, M. Bechelany, J. M. Janot and S. Balme, *Microchim. Acta*, 2014, 1-7.
20 Y. Liu, Y. Liu, M. Zhou, K. Huang, J. Cao, H. Wang and Y. Chen, *J. Chromatogr. A*, 2014, **1340**, 128-133.
21 G. Lu, P. Tan, C. Lei, Z. Nie, Y. Huang and S. Yao, *Talanta*, 2014, **128**, 360-365.
22 S. L. Ting, S. J. Ee, A. Ananthanarayanan, K. C. Leong and P. Chen, *Electrochim. Acta*, 2015, DOI:10.1016/j.electacta.2015.01.026.
23 W. Chen, F. Cao, W. Zheng, Y. Tian, Y. Xianyu, P. Xu, W. Zhang, Z. Wang, K. Deng and X. Jiang, *Nanoscale*, 2015, **7**, 2042-2049.
24 W. Qi, J. Zhao, W. Zhang, Z. Liu, M. Xu, S. Anjum, S. Majeed and G. Xu, *Anal. Chim. Acta*, 2013, **787**, 126-131.
25 H. K. Kweon and K. Hakansson, *Anal. Chem.*, 2006, **78**, 1743-1749.
26 Z. Amghouz, C. A. Azpilicueta, K. Burusco, J. García, S. Khainakov, A. Luquin, R. Nieto and J. Garrido, *Micropor. Mesopor. Mat.,* 2014, **197**, 130-139.
27. P. Tan, C. Lei, X. Liu, M. Qing, Z. Nie, M. Guo, Y. Huang and S. Yao, *Analytica Chimica Acta*, 2013, **780**, 89-94.
28 T. Yin, H. Li, N. Yang, T. Gao, L. Sun and G. Li, *Biosens. Bioelectron.*, 2014, **56**, 1-5.
29 D. H. Hua, W. C. Lin, L. A. Lin, L. G. Wen, C. Wei and L. X. Hua, *Sensor. Actuat. B-Chem.*, 2014, **191**, 479-484.
30 J. Zhang, Y. Liu, J. Lv and G. Li, *Nano Res.*, 2014, **8**, 920-930.
31 T. Gao, L. Ning, C. Li, H. Wang and G. Li, *Anal. Chim. Acta*, 2013, **788**, 171-176.
32 X. Zhu, Y. Liu, J. Yang, Z. Liang and G. Li, *Biosens. Bioelectron.*, 2010, **25**, 2135-2139.
33 Y. Chen, J. Zhang, Y. Gao, J. Lee, H. Chen and Y. Yin, *Biosens. Bioelectron.,* 2015, DOI:10.1016/j.bios.2015.04.036.
34 W. Yang, Y. He, L. Xu, D. Chen, M. Li, H. Zhang and F. Fu, *J. Mater. Chem.*, 2014, **2**, 7765-7770.
35 C. H. Hong, Y. Xiang, D. Hai, C. Jiye and Y. P. Hui, *J. Food Eng.*, 2014, **142**, 163-169.
36 S. Zhan, H. Xu, X. Zhan, Y. Wu, L. Wang, J. Lv and P. Zhou, *Microchim. Acta*, 2015, 1-9.
37 M. R. Nezhad and S. A. Moayed, *Plasmonics*, 2015, 1-8.
38 M. Yu, *Aust. J. Chem.*, 2014, **67**, 813-818.
39 Z. Guo, X. Niu, T. Xiao, J. Lu, W. Li and Y. Zhao, *J. Funct. Foods*, 2015, **14**, 324-336.
40 M. R. Kandadi, E. Panzhinskiy, N. D. Roe, S. Nair, D. Hu and A. Sun, *BBA-Mol. Basis Dis.,* 2015, **1852**, 299-309.
41 N. P. Hung, B. T. Zhao, M. Y. Ali, J. S. Choi, D. Y. Rhyu, B. S. Min and M. H. Woo, *J. Nat. Prod.*, 2015, **78**, 34-42.
42 Y. S. Shim, K. C. Kim, D. Y. Chi, K.H. Lee and H. Cho, *Bioorg. Med. Chem. Lett.*, 2003, **13**, 2561-2563.
43 D. Li, W. Li, K. Higai and K. Koike, *J. Nat. Med.*, 2014, **68**, 427-431.
41 W. Zhang, D. Hong, Y. Zhou, Y. Zhang, Q. Shen, J. Y. Li, L. H. Hu and J. Li, *BBA-Gen. Subjedcts*, 2006, **1760**, 1505-1512.
42 S. M. Stanford, V. Ahmed, A. M. Barrios and N. Bottini, *Antioxid. Redox Sign.* 2014, **20**, 2160-2178.
43 G. Huyer, S. Liu, J. Kelly, J. Moffat, P. Payette, B. Kennedy, G. Tsaprailis, M. J. Gresser and C. Ramachandran, *J. Biol. Chem.*, 1997, **272**, 843-851.